Commun. Comput. Phys.
doi: 10.4208/cicp.101114.150415a

Vol. **18**, No. 3, pp. 757-786
September 2015

Lattice Boltzmann Simulation of Particle Motion in Binary Immiscible Fluids

Yu Chen[1], Qinjun Kang[2], Qingdong Cai[3,*], Moran Wang[1,*] and Dongxiao Zhang[4]

[1] *Department of Engineering Mechanics and CNMM, School of Aerospace, Tsinghua University, Beijing 100084, China.*
[2] *Earth and Environmental Sciences Division, Los Alamos National Laboratory, Los Alamos, New Mexico 87545, USA.*
[3] *LTCS, CAPT and Department of Mechanics and Aerospace Engineering, Peking University, Beijing 100871, China.*
[4] *Department of Energy and Resources Engineering, Peking University, Beijing, China.*

Received 10 November 2014; Accepted (in revised version) 15 April 2015

Abstract. We combine the Shan-Chen multicomponent lattice Boltzmann model and the link-based bounce-back particle suspension model to simulate particle motion in binary immiscible fluids. The impact of the slightly mixing nature of the Shan-Chen model and the fluid density variations near the solid surface caused by the fluid-solid interaction, on the particle motion in binary fluids is comprehensively studied. Our simulations show that existing models suffer significant fluid mass drift as the particle moves across nodes, and the obtained particle trajectories deviate away from the correct ones. A modified wetting model is then proposed to reduce the non-physical effects, and its effectiveness is validated by comparison with existing wetting models. Furthermore, the first-order refill method for the newly created lattice node combined with the new wetting model significantly improves mass conservation and accuracy.

PACS: 47.11.Qr, 47.55.-t, 47.56.+r, 47.57.Gc, 47.61.Jd

Key words: Lattice Boltzmann model, particle suspension model, binary immiscible fluids.

1 Introduction

Particle suspension in multiphase or multicomponent flows has gained increasing attention during the last decade [3, 4, 16, 20, 23, 24, 28, 32, 41, 42], due to the extensive use

*Corresponding author. *Email addresses:* caiqd@pku.edu.cn (Q. Cai), mrwang@tsinghua.edu.cn (M. Wang), fishfrozen@gmail.com (Y. Chen), qkang@lanl.gov (Q. Kang), donzhang01@gmail.com (D. Zhang)

 ©2015 Global-Science Press

https://doi.org/10.4208/cicp.101114.150415a Published online by Cambridge University Press

of particles to stablize emulsions, which has many applications in food, cosmetics and medical industires [23], as well as the use of proppants in hydraulic fracturing for unconventional gas production [36]. Also, in many processes, such as hydrocarbon recovery, geologic CO_2 sequestration, and soil wetting and drying, understanding the emergent patterns of the invasion of one fluid into a deformable porous medium filled with another fluid is both scientifically fascinating and technologically important [21]. If the deformable porous medium is modeled by the discrete element method [14], then it all boils down to the problem of accurately simulating particle suspension in multiphase or multicomponent flow.

Numerical simulation of particle suspension in multiphase or multicomponent flows requires accurately capturing the motion of particle and the interface of the fluid, neither of which can be easily accomplished by traditional CFD method. The lattice Boltzmann method (LBM) has become a powerful numerical tool to model complex flow and multi-physicochemical transport processes [1,9,43,44], and is suitable to fulfill the above requirements, mainly due to the fact that it is based on microscopic models and mesoscopic kinetic equations [9]. It has already been employed to simulate particle suspension in multiphase or multicomponent flows [16,23,24,28,32,41,42]. The link-based lattice Boltzmann particle suspension model, first proposed by Ladd [26] and further developed by Aidun *et al.* [2], has been widely used and the LBM simulation results are comparable to the finite element results [11,34]. For modeling multiphase or multicomponent flow, the Shan-Chen pseudo-potential lattice Boltzmann model [8,33,37–39] has been applied with considerable success [1]. In this paper, we combine the link-based particle suspension model and the classic Shan-Chen multicomponent model [38] to simulate particle suspension in binary immiscible fluids.

Previous LBM approaches have reported mass non-conservation issue [23,41] when the fluid information inside the particle is excluded. Although retaining fluid information inside the particle can ensure exact mass conservation in the whole computation domain including the solid particle region [24, 28, 32], the fluid mass may not be conserved in the fluid region outside the particle. Also, when introducing non-neutral wetting, additional wetting forces will act on the solid particle, and nonphysical effects such as density variations near solid surface affect the motion of the particle. Simulation accuracy may be decreased compared with single phase flow simulations, which has not been well studied. Therefore, in this paper, we will focus on the accuracy and mass conservation of the existing approaches, and propose a modified approach to reduce mass non-conservation and to improve accuracy.

The rest of the paper is organized as follows. Section 2 introduces the numerical methods of this paper, including the Shan-Chen multicomponent model, particle suspension model and related modifications required in combining these two models. In Section 3, we perform extensive numerical simulations to validate our method and compare the results with existing methods. Section 4 concludes the paper.

https://doi.org/10.4208/cicp.101114.150415a Published online by Cambridge University Press

2 Numerical methods

2.1 Shan-Chen multicomponent lattice Boltzmann model

In the Shan-Chen multicomponent model [38,39], each fluid component k is represented by its own distribution functions, which follow the similar LBGK [7,35] evolution equation as in single phase flow,

$$f_i^k(\boldsymbol{x}+\boldsymbol{e}_i\delta t,t+\delta t)=f_i^k(\boldsymbol{x},t)-\frac{f_i^k(\boldsymbol{x},t)-f_i^{k(eq)}(\boldsymbol{x},t)}{\tau^k}, \tag{2.1}$$

where f_i^k is the distribution function of component k associated with the ith discrete velocity direction $\boldsymbol{e}_i$, $f_i^{k(eq)}$ is the corresponding equilibrium distribution function, δt is the time increment and τ^k is the relaxation time, which relates to the kinematic viscosity of fluid component k. For the popular D2Q9 lattice model, the equilibrium distribution functions are chosen as [25],

$$f_i^{k(eq)}(n_k,\boldsymbol{u}_k^{eq})=\begin{cases}\alpha_k n_k-\frac{2}{3}n_k\boldsymbol{u}_k^{eq}\cdot\boldsymbol{u}_k^{eq}, & \text{if } i=0;\\ \frac{(1-\alpha_k)n_k}{5}+\frac{1}{3}n_k(\boldsymbol{e}_i\cdot\boldsymbol{u}_k^{eq})+\frac{1}{2}n_k(\boldsymbol{e}_i\cdot\boldsymbol{u}_k^{eq})^2-\frac{1}{6}n_k\boldsymbol{u}_k^{eq}\cdot\boldsymbol{u}_k^{eq}, & \text{if } i=1,\cdots,4;\\ \frac{(1-\alpha_k)n_k}{20}+\frac{1}{12}n_k(\boldsymbol{e}_i\cdot\boldsymbol{u}_k^{eq})+\frac{1}{8}n_k(\boldsymbol{e}_i\cdot\boldsymbol{u}_k^{eq})^2-\frac{1}{24}n_k\boldsymbol{u}_k^{eq}\cdot\boldsymbol{u}_k^{eq}, & \text{if } i=5,\cdots,8,\end{cases} \tag{2.2}$$

where α_k is a free parameter, which relates to the sound speed of a region of pure kth component as $(c_s^k)^2=\frac{3}{5}(1-\alpha_k)$; n_k is the number density of kth component,

$$n_k=\sum_i f_i^k. \tag{2.3}$$

$\boldsymbol{u}_k^{eq}$ is the 'equilibrium velocity', by which the forcing term is incorporated,

$$\rho_k\boldsymbol{u}_k^{eq}=\rho_k\boldsymbol{u}'+\tau_k\boldsymbol{F}_k. \tag{2.4}$$

where $\boldsymbol{u}'$ is a common velocity on top of which, an extra component-specific velocity due to interparticle interaction is added for each component [22]. The forcing term in Eq. (2.4) includes the fluid-fluid interactive force F_{ffk} between different components, the fluid-solid interactive force F_{fsk} and the body force F_{bk} [25]. The density and velocity of each component can be obtained by the following equations,

$$\rho_k=m_k n_k=m_k\sum_i f_i^k, \tag{2.5}$$

$$\rho_k\boldsymbol{u}_k=m_k n_k\boldsymbol{u}_k=m_k\sum_i f_i^k\boldsymbol{e}_i, \tag{2.6}$$

where m_k is the molecular mass of k the component. The macroscopic bulk velocity $\boldsymbol{u}$ is defined by [18,40],

$$\rho\boldsymbol{u}=\sum_{k=1}^{s}\rho_k\boldsymbol{u}_k+\frac{1}{2}\sum_{k=1}^{s}\rho_k\boldsymbol{F}_k. \tag{2.7}$$

https://doi.org/10.4208/cicp.101114.150415a Published online by Cambridge University Press

2.1.1 Fluid-fluid interactive force

In order to simulate separation between different components in multicomponent fluids, non-local interactions between fluid particles are incorporated via the following fluid-fluid interactive force [38],

$$F_{ffk}(\boldsymbol{x}) = -\psi_k(\boldsymbol{x}) \sum_{\boldsymbol{x}'} \sum_{\overline{k}=1}^{s} G_{k\overline{k}}(\boldsymbol{x},\boldsymbol{x}') \psi_{\overline{k}}(\boldsymbol{x}')(\boldsymbol{x}'-\boldsymbol{x}), \tag{2.8}$$

where $F_{ffk}(\boldsymbol{x})$ is the total fluid-fluid interactive force on the kth component, $G_{k\overline{k}}(\boldsymbol{x},\boldsymbol{x}')$ is the interparticle potential which satisfies $G_{k\overline{k}}(\boldsymbol{x},\boldsymbol{x}') = G_{\overline{k}k}(\boldsymbol{x},\boldsymbol{x}')$, and $\psi_k(\boldsymbol{x})$ is the effective number density for kth component. For simplicity, ψ_k is taken as n_k in this study. Other choices will give a different equation of state [22].

In the D2Q9 model, $G_{k\overline{k}}(\boldsymbol{x},\boldsymbol{x}')$ can be written as,

$$G_{k\overline{k}}(\boldsymbol{x},\boldsymbol{x}') = \begin{cases} g_{k\overline{k}}, & \text{if } |\boldsymbol{x},\boldsymbol{x}'| = \delta x; \\ g_{k\overline{k}}/4, & \text{if } |\boldsymbol{x},\boldsymbol{x}'| = \sqrt{2}\delta x; \\ 0, & \text{otherwise.} \end{cases} \tag{2.9}$$

Here $g_{k\overline{k}}$ controls the strength of interparticle potential of component k and component $\overline{k}$, which related to the surface tension. $g_{k\overline{k}}$ is a positive value so that different immiscible fluid components repel with each other. However, the Shan-Chen model is not a strictly immiscible model, as there is always a small amount of fluid component $\overline{k}$ inside the fluid component k region [22]. This slightly mixing feature of the Shan-Chen model may affect the motion of the particle suspended in the multicomponent fluids, and will be investigated numerically in Section 3.

2.1.2 Fluid-solid interactive force: Wettability

When solid phase exists in the simulation domain of multicomponent fluids, an interactive force between the solid and the fluid is introduced in order to control the contact angle on the solid/fluid interface. Martys and Chen [29] proposed the following fluid-solid interactive force, referred as the Martys model, which has been widely used with the Shan-Chen multicomponent model,

$$F_{fsk}(\boldsymbol{x}) = -n_k(\boldsymbol{x}) \sum_i g_{kw} s(\boldsymbol{x}+\boldsymbol{e}_i)\boldsymbol{e}_i, \tag{2.10}$$

where $s(\boldsymbol{x}) = 1$ represents solid node and $s(\boldsymbol{x}) = 0$ represents fluid node. g_{kw} can be used to control the relative wettability of different fluid components. For example, wetting fluid has a negative g_{kw} value while non-wetting fluid has a positive g_{kw} value. One may expect that fluid near the solid surface is attracted to the solid surface for wetting fluid or repelled by the solid surface for non-wetting fluid. However, even if $F_{fsk}(\boldsymbol{x}) = 0$, which results in a 90° contact angle, fluid near the solid surface is still attracted to the solid surface.

https://doi.org/10.4208/cicp.101114.150415a Published online by Cambridge University Press

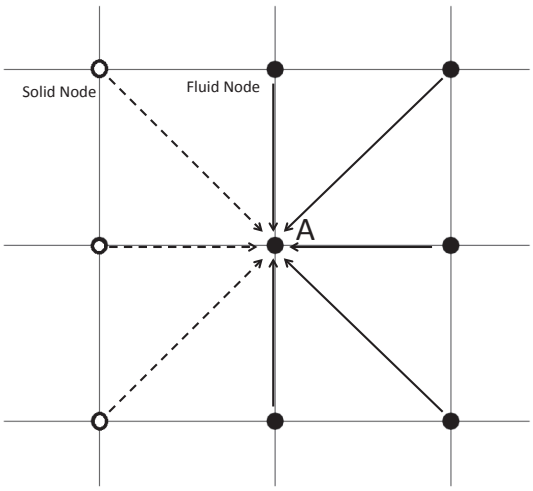


Figure 1: A schematic illustration of fluid-solid boundary nodes in D2Q9 lattices.

As shown in Fig. 1, node A is a fluid node near solid surface, so called fluid boundary node, and is connected with solid nodes. Fluid particles on node A experience repellent fluid-fluid interactive forces, as shown in Eq. (2.8), from other fluid components on the nearby fluid nodes, and since some links of node A are connected with solid nodes, the net fluid-fluid interactive force on node A is towards the solid surface. Therefore, even if the fluid-solid interactive force is zero, fluid near the solid surface is still attracted to the solid surface.

The lattice Boltzmann method is not a strictly incompressible model [9]. If the fluid on the boundary nodes experiences, for example, a net interactive force towards the solid surface, the local fluid density of the boundary nodes will be higher than nearby non-boundary nodes, as the fluid particles are attracted to the solid surface. On the other hand, if the net interactive force is towards the fluid domain, then the local fluid density of the boundary nodes will be lower than nearby non-boundary nodes, as the fluid particles are pulled away from the solid surface. This density variations near the solid surface are also observed in Ref. [23], and can affect the motion of the particle suspended in the fluid, as we will demonstrate in Section 3. The compressible effect is one of the drawbacks of LBM. Although several incompressible single phase LB models have been proposed [17, 19, 49], based on our understanding, one can only reduce this effect but cannot completely eliminate it especially in multicomponent flow simulations.

In the Martys model, the net force on the boundary nodes is the sum of F_{ffk} and F_{fsk}, and F_{ffk} is usually much larger than F_{fsk} in practice. Thus, the density variations on the fluid boundary nodes can be significant, especially for the wetting fluid component, as F_{ffk} and F_{fsk} are in the same direction.

In order to overcome the above problem, Jansen and Harting [23] proposed a new wetting model, referred as the Jansen model, which employs virtual fluid on the solid

https://doi.org/10.4208/cicp.101114.150415a Published online by Cambridge University Press

boundary nodes to balance the net fluid-fluid interactive force on the fluid boundary nodes. As shown in Fig. 1, solid boundary nodes are now filled with virtual fluid of each component. The density of the virtual fluid is the average fluid density of the surrounding fluid nodes,

$$n^{avg}_{k(virtual)}(\boldsymbol{x},t)=\frac{1}{N_{NP}}\sum_{i_{NP}} n_k(\boldsymbol{x}+\boldsymbol{e}_{i_{NP}},t), \tag{2.11}$$

where NP refers to fluid node that directly connect to the corresponding solid boundary node. Thus, the net interactive force on the boundary nodes becomes negligible thanks to the counterbalance provided by the virtual fluid on the solid boundary nodes, and the density variations vanish when the contact angle is 90°. For contact angle not equal to 90°, a small amount of additional virtual fluid of the wetting component is added to the solid boundary nodes while the density of the non-wetting component on the solid boundary nodes remains the same as in Eq. (2.11),

$$n_{w(virtual)}=n^{avg}_{w(virtual)}+|\Delta s|, \tag{2.12a}$$

$$n_{nw(virtual)}=n^{avg}_{nw(virtual)}, \tag{2.12b}$$

where w represents wetting component and nw represents non-wetting component. In such case, the repulsion between the increased component (wetting component) and the unmodified one (non-wetting component) increases, making the solid surface push away the non-wetting component and 'prefer' the wetting component [23]. In the Jansen model, Eq. (2.10) is no longer used, and the fluid-solid interactive forces are obtained by calculating the fluid-fluid interactive forces between fluid boundary nodes and virtual fluid nodes via Eq. (2.8). The density variations still exist on fluid boundary nodes as long as the extra virtual fluid in Eq. (2.12) is added to the solid boundary nodes, which breaks the balance of fluid-fluid interactive forces on the fluid boundary nodes. The magnitude of the variations is smaller than when using the Martys model, but not negligible, which will affect the motion of the suspended particle.

In the Jansen model, only the virtual fluid density of the wetting component is modified, which affects the interactive forces acting on the non-wetting component on the fluid boundary nodes. The magnitude of the counterforces of the fluid-solid interactive forces that exert on a solid particle as well as the magnitude of the density variations near the particle surface are much larger when the particle is submerged in the non-wetting component than those when the particle is submerged in the wetting component. As a result, the simulated particle motion may be less accurate when the particle is submerged in the non-wetting component.

We notice that the virtual fluid is only used in Eq. (2.8) to control the nonlocal interactive forces on the fluid boundary nodes, and will not enter the fluid domain to take part in the standard LBM streaming-collision procedure. In other words, the density of the virtual fluid can be regarded as merely a parameter to control the wettability of the corresponding fluid component. Therefore, a negative value for the virtual fluid density

https://doi.org/10.4208/cicp.101114.150415a Published online by Cambridge University Press

is acceptable. We propose the following modified wetting model,

$$n^{new}_{k(virtual)} = n^{avg}_{k(virtual)} + \Delta s_k. \tag{2.13}$$

Here Δs_k can be any value, and we choose to let $\Delta s_{wetting} = -\Delta s_{non-wetting} = \Delta s$ in current study, where Δs is a positive value. In such case, the solid particle experience similar fluid-solid interactive forces either when it is submerged in wetting component or when it is submerged in non-wetting component. Also, the density variations on the fluid boundary nodes in either fluid component are in the same level. Thus, the simulation results of the particle submerged in different components should be more consistent.

2.2 Particle suspended in multicomponent fluids

In the Shan-Chen multicomponent lattice Boltzmann model, different component is represented by its own distribution functions [38]. Particle suspended in multicomponent fluids can be treated similarly as in single phase fluid for each individual fluid component, except that additional fluid-solid interactive force is applied to the particle.

2.2.1 Interior fluid

There are two types of particle suspension models depending on whether fluid information inside the particle is excluded or not. For particle suspension model with interior fluid, the fluid information is stored on all the lattice nodes including those in the solid region. Thus, for a single component fluid, when the particle moves across lattice nodes, the total mass of the fluid is strictly conserved. However, when the particle is suspended in multicomponent fluids, how to define the composition of the fluid components inside the particle becomes a problem, because when the particle is penetrating the interface of two fluid components, some fluid components will enter the particle while some will leak out of the particle. Although the total fluid mass of each component is strictly conserved, the mass of each fluid component in the fluid region is not conserved, and the components composition in the fluid region drifts. We demonstrated in Section 3.3 that using the particle suspension model with interior fluid results in significant fluid components composition drift outside the particle, as shown in Fig. 8. Thus, in this study, we choose to exclude the interior fluid. Readers shall keep in mind that the virtual fluid in the wetting model is not considered as interior fluid, because the virtual fluid does not enter the fluid domain to take part in the standard LBM streaming-collision procedure.

2.2.2 Non-slip boundary condition

In this paper, we mainly focus on the link-based non-slip boundary conditions, which are widely used in LB simulations of particle-fluid interactions [2, 26, 31]. Fig. 2 shows the typical link-based boundary model. In link-based boundary models, fluid interacts with solid through boundary links, such as link AC in Fig. 2 which connects a fluid node A and a solid node C.

https://doi.org/10.4208/cicp.101114.150415a Published online by Cambridge University Press

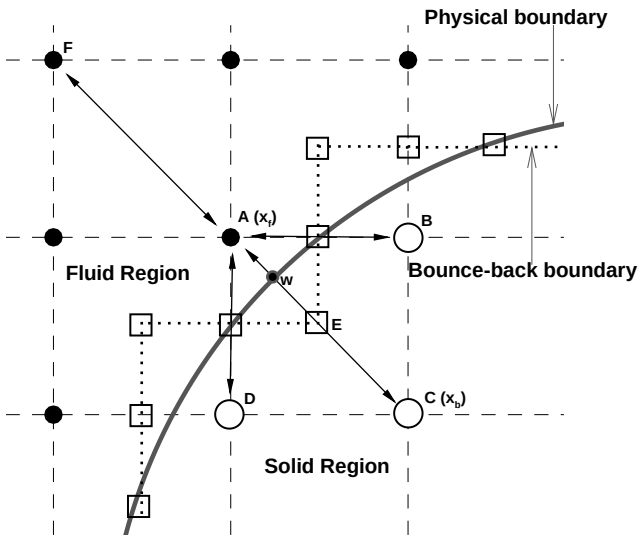


Figure 2: A schematic illustration of link-based lattice Boltzmann boundary model.

Classic particle suspension models employ the midway bounce-back boundary condition [26],

$$f_{\tilde{\alpha}}(\boldsymbol{x}_f, t+\Delta t) = \tilde{f}_{\alpha}(\boldsymbol{x}_f, t) - 2\omega_{\alpha}\rho\frac{\boldsymbol{e}_{\alpha}\cdot\boldsymbol{u}_w}{c_s^2}, \tag{2.14}$$

where $\boldsymbol{x}_f$ is the location of the fluid boundary node, $\boldsymbol{e}_{\alpha}$ is the lattice direction from fluid node to solid node, $\boldsymbol{e}_{\tilde{\alpha}}$ is the opposite direction, $\tilde{f}$ is the post collision distribution function and $\boldsymbol{u}_w$ is the wall velocity evaluated on the mid-point of the boundary link. For particle suspended in multi-component fluids, each fluid component collide with the solid wall under the same bounce-back rule as in Eq. (2.14).

The drawback of the midway bounce-back boundary condition is that the resulting non-slip boundary is a zigzag type boundary as shown in Fig. 2, and is only first-order accurate for arbitrary surface. Higher-order interpolation based curved boundary conditions have been proposed to improve the accuracy [5,12,15,27,30,47,48], which utilize the exact wall position (point W in Fig. 2), and interpolate required information from nearby fluid nodes. However, even if a curved boundary condition is applied, existing wetting models do not account for the exact wall position which will degrade the accuracy of the curved boundary conditions. Also, our simulation results of particle sedimentation [11] show that the mid-way bounce-back boundary condition is able to produce simulation results with acceptable accuracy as long as the grid resolution of the particle is fine enough. Therefore, only the mid-way bounce-back boundary condition is used in this work.

https://doi.org/10.4208/cicp.101114.150415a Published online by Cambridge University Press

2.2.3 Particle dynamics

Particle suspended in multicomponent fluids not only experiences the hydrodynamic forces from the surrounding fluids, but also experiences the counterforces of the fluid-solid interactive forces acting on the fluid boundary nodes. Readers shall keep in mind that the absolute value of the fluid-solid interactive forces has no physical meaning, but the relative value of the fluid-solid interactive force keeps the particle suspended on the interface with desired contact angle.

The hydrodynamic force of each component acting on the solid surface can be obtained by the classic momentum exchange method,

$$\delta \boldsymbol{F}_w^k(\boldsymbol{x}_w,\boldsymbol{e}_\alpha) = -\left[f_{\bar{\alpha}}^k(\boldsymbol{x}_f,t)\boldsymbol{e}_{\bar{\alpha}} - \tilde{f}_\alpha^k(\boldsymbol{x}_f,t)\boldsymbol{e}_\alpha\right]. \tag{2.15}$$

When the mid-way bounce-back boundary condition is applied, Eq. (2.15) can be written as,

$$\delta \boldsymbol{F}_w^k(\boldsymbol{x}_w,\boldsymbol{e}_\alpha) = \left[2\tilde{f}_\alpha^k(\boldsymbol{x}_f,t) - 2\omega_\alpha \rho_k \frac{\boldsymbol{e}_\alpha \cdot \boldsymbol{u}_w}{c_s^2}\right]\boldsymbol{e}_\alpha. \tag{2.16}$$

As pointed out in Ref. [11], the classic momentum exchange method does not account for the initial momentum of the net mass transfer term $-2\omega_\alpha\rho_k\frac{\boldsymbol{e}_\alpha\cdot\boldsymbol{u}_w}{c_s^2}$ in Eq. (2.14), and an impulse correction has to be applied to the particle whenever the particle moves to cover or uncover a fluid lattice nodes as the momentum of the fluid on these nodes is gained or lost by the particle [2], respectively,

$$\boldsymbol{F}_c(\boldsymbol{x}_{cover}) = \sum_{k=1}^{s}\sum_{i=1}^{8} f_i^k(\boldsymbol{x}_{cover})\boldsymbol{e}_i, \tag{2.17}$$

$$\boldsymbol{F}_u(\boldsymbol{x}_{uncover}) = \sum_{k=1}^{s}\sum_{i=1}^{8} f_i^k(\boldsymbol{x}_{uncover})\boldsymbol{e}_i. \tag{2.18}$$

Although several corrected momentum exchange methods [6, 11, 13, 45] have been proposed to correct the classic momentum exchange method directly in Eq. (2.15), without the need of the impulse force correction which results in a fluctuating force, our early test results show that none of the corrected momentum exchange methods works well when the contact angle is not equal to 90°. The reason may be that the alteration of distribution functions on the fluid boundary nodes due to the non-zero interactive force in Eq. (2.4) renders some assumptions in the development of the corrected momentum exchange methods invalid, while the impulse correction ignores the complex interactions between fluid and solid during the process of particle covering/uncovering fluid nodes, and only the final momentum of the fluid on these nodes is accounted for.

The counterforce of the fluid-solid interactive force, denoted as $F_{sfk}(\boldsymbol{x}_b)$, is acting on the corresponding solid boundary node $\boldsymbol{x}_b$. This interactive force described above is considered as an artificial model to simulate desired contact angle and can not be directly

https://doi.org/10.4208/cicp.101114.150415a Published online by Cambridge University Press

related to the physical interaction between solid and fluid. When a solid particle is submerged entirely in one fluid component, the integration of $F_{sfk}(\boldsymbol{x}_b)$ on the particle surface should be zero. However, due to the discrete lattice structure and the density variations caused by the compressible effect of the LBM, the particle will experience a small net force formed from the fluid-solid interactive forces, which will affect the particle motion. One of the main reasons of the new wetting model proposed in Section 2.1.2 is to reduce the impact of the above artificial net force as well as the density variations on the particle motion.

Once the total force and torque on the particle is obtained, the position and velocity of the rigid particle can be updated according to Newton's law.

2.2.4 Refill procedure

When the particle moves across lattice nodes, some lattice nodes originally inside the particle will enter the fluid domain. Because the interior fluid is excluded, fluid information is unknown in those newly created fluid nodes, and therefore a refill procedure is required. There are several refill methods, such as using the average surrounding fluid density and the rigid body velocity for the new node and replacing the distribution functions with the equilibrium distribution functions [2], or one can just directly use the averaged extrapolation values of the distribution functions from nearby fluid nodes [10, 46].

We find that the difference between using the extrapolation of macroscopic density and using the direct extrapolation of the distribution functions is negligible. In this work, we choose to use the direct extrapolation of the distribution functions for the new lattice nodes, unless stated otherwise.

The extrapolation scheme can either be a zero-order scheme or a first-order scheme. Although the difference between the zero-order refill and the first-order refill is very small in single phase simulations as the gradient of the fluid density near the solid surface is small, this may not be true in the multiphase/multicomponent simulations. As shown in Section 2.1.2 and Section 3.2, there are density variations near the solid surface caused by the wetting models. The reconstruction of the newly created lattice nodes must consider the effects of the density variations which alter the gradient of the fluid density near the solid surface.

For the newly created lattice nodes near the triple contact line, first-order extrapolated fluid distribution functions can be extremely large or be negative due to the large density variations across the fluid interface, which results in nonphysical phase separation near the solid surface or unstable simulations. The problem can be solved, by simply employing a criterion in the extrapolations. If the first-order extrapolated fluid density is smaller than zero, or the magnitude of the nearby density variation is larger than certain criterion, such as 0.1 in lattice unit based on the parameters in the Shan-Chen model, then the zero-order extrapolation scheme kicks in to replace the first-order extrapolation scheme. We will investigate both the zero-order refill and the first-order refill in Section 3.4.

https://doi.org/10.4208/cicp.101114.150415a Published online by Cambridge University Press

3 Numerical validation

Our code for the LB simulation of particle suspension in a single phase fluid was validated in [11], by comparison with the finite element method. For the numerical simulation of particle suspension in multicomponent flows, it is difficult to quantitatively compare the simulation results with experiment results, due to complex interactions between different fluid components as well as interactions between solid particle and multiple fluid components. However, for a numerical model to be valid, at least the following requirements should be met:

(1) When a particle is completely submerged in one of the fluid components, particle trajectory obtained by the multicomponent code should be close to the one obtained by the single phase code, as long as the particle is far away from fluid interface;

(2) When a particle is suspended on the interface of two fluid components, the final static contact angles determined by the stable position of the particle, under the condition of zero gravity, should be consistent with the contact angles formed by a flat solid surface in contact with these two fluid components, as shown in Fig. 3;

(3) The mass composition of the multicomponent fluid should remain constant if no chemical reaction occurs.

In the following sections, we first obtained the parameters of different wetting models to form an identical contact angle for valid comparison between these models. Then the density variations near solid surface caused by the wetting models were investigated. In order to validate objective (1), we simulated the sedimentation of an elliptical particle using our multicomponent LB code and took account of the non-physical effects of the wetting models and the non-strictly immiscible nature of the Shan-Chen model, while assuming the fluid interface is infinitely far away. Finally, three dimensional simulations of particle suspended on the fluid interface were performed to examine whether the forces exerted on the solid particle correctly reproduce desired contact angle.

3.1 Determining the parameters of different wetting models

Three wetting models, the Martys model, the Jansen model and the present model, are introduced in Section 2.1.2. The contact angle cannot be determined prior to numerical simulation for these wetting models. In order to perform valid comparison between these wetting models, we adjust the parameters in the wetting models and perform simulations to form an identical contact angle.

The 2D simulation domain is a 301×201 closed cavity, with non-slip bounce-back boundary condition applied to the domain boundaries. For simplicity, two immiscible fluid components, fluid R and fluid B, with identical viscosity and density are studied. We let $\tau_R=\tau_B=1$, $m_R=m_B=1$ and the interparticle potential coefficient $g_{RB}=0.2$.

https://doi.org/10.4208/cicp.101114.150415a Published online by Cambridge University Press

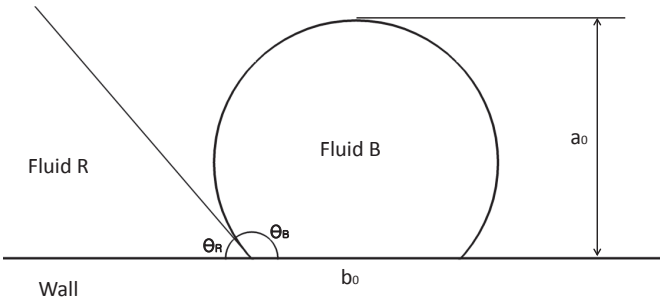


Figure 3: A schematic illustration of calculating contact angle.

A fluid B drop is attached to one of the flat walls, as shown in Fig. 3. The contact angle can be calculated by the following equations [25],

$$R=\frac{a_0}{2}+\frac{b_0^2}{8a_0}, \tag{3.1}$$

$$\tan(\theta_B)=\frac{b_0}{2(R-a_0)}, \tag{3.2}$$

where R is the radius of curvature of the drop.

In this case, we adjusted the parameters in the wetting models to form an identical contact angle, $\theta_B=119^\circ$. Table 1 shows the obtained parameters for each wetting models, which will be used in the following comparisons.

Table 1: Parameters.

Models	Martys *et al*. [29]	Jansen *et al*. [23]	present model
Parameters	$g_{Rw}=-0.022$ $g_{Bw}=0.022$	$\Delta s_R=0.225$ $\Delta s_B=0$	$\Delta s_R=0.104$ $\Delta s_B=-0.104$
Contact Angle (Fluid R)	61°	61°	61°
Contact Angle (Fluid B)	119°	119°	119°

3.2 Density variations caused by the wetting models

When the contact angle is not equal to 90°, the fluid boundary nodes experience non-zero net interactive forces from surrounding solid nodes and fluid nodes, which causes density variations on these fluid boundary nodes. Here we investigate density variations on stationary walls. As shown in Fig. 4, the simulation domain is a 201×101 cavity, with non-slip bounce-back boundary condition applied to the domain boundaries. The cavity is filled with two immiscible fluids, fluid R and fluid B, each occupying half of

https://doi.org/10.4208/cicp.101114.150415a Published online by Cambridge University Press

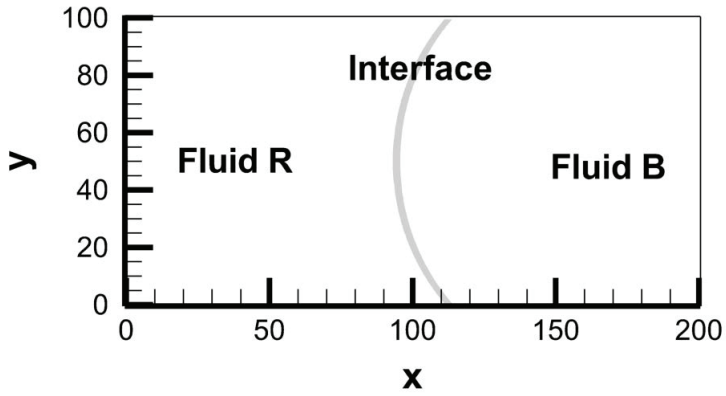


Figure 4: The simulation domain for the study of the density variations near stationary walls. Fluid interface is in the middle of the cavity.

the domain. The parameters of the fluids are identical to the ones used in Section 3.1. In Section 2.1, we have pointed out that the Shan-Chen model is not a strictly immiscible model [22]. Thus, in fluid R region, the dominant fluid component is fluid R, while there also exists a small amount of fluid B in fluid R region, the so called residual component. In fluid B region, the dominant component is fluid B, and the residual component is fluid R.

Fig. 5 shows the density profile of the corresponding dominant component near the left and right wall along the line $y=50$, respectively. Fig. 6 shows the density profile of the corresponding residual component near the left and right wall along the line $y=50$, respectively. We can see obvious density variations near the wall caused by the wetting models.

In the Martys model, the fluid-fluid interactive force is not balanced on the boundary nodes, thus the density variation of the non-wetting fluid near the wall is very large, as shown in Fig. 5b. In Fig. 5a, the density of the second node ($x=1.5$) is smaller than the first node ($x=0.5$) and the third node ($x=2.5$). The reason is that, in the Martys model, the net interactive force on the residual component on the fluid boundary nodes is always towards the wall even when the residual component is the non-wetting component, because the net force of the fluid-fluid interactive forces from the surrounding fluid nodes is towards the solid surface and usually larger than the net force of the fluid-solid interactive forces in Eq. (2.10). The density of the residual component on the boundary nodes is therefore always higher than the fluid nodes further away from the wall. As shown in Fig. 6a, the residual component (fluid B, non-wetting component) density on the first node is relatively high, and push away the dominant fluid R on the second node, resulting in slightly lower density of fluid R on the second node, as shown in Fig. 5a.

The patterns of the density profiles of the Jansen model and the present model are similar and less complex, as both models employ the virtual fluid to balance the fluid-

https://doi.org/10.4208/cicp.101114.150415a Published online by Cambridge University Press

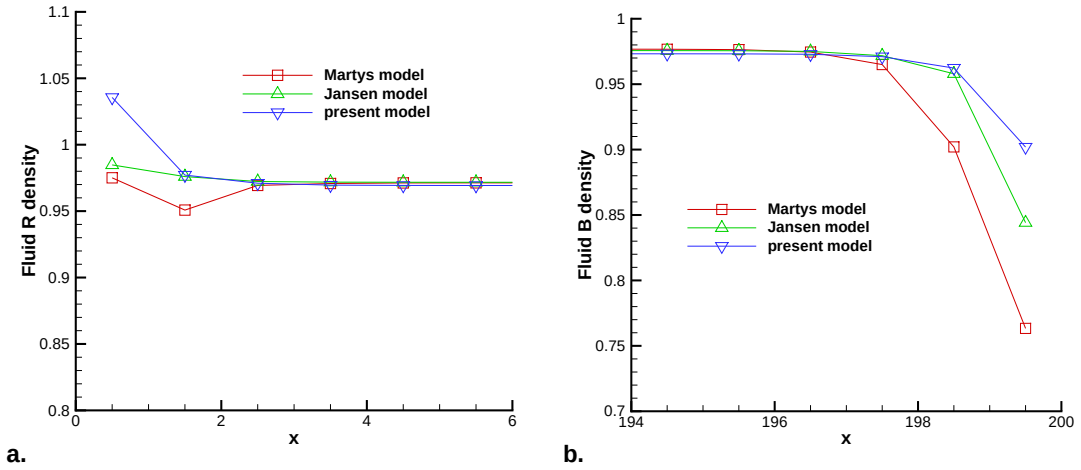


Figure 5: (Color online) The density profile of the dominant fluid component near the wall along $y=50$. (a) The density profile of fluid R near the left wall. In this region, the wetting fluid R is the dominant component while the non-wetting fluid B is the residual component. (b) The density profile of fluid B near the right wall. In this region, the non-wetting fluid B is the dominant component while the wetting fluid R is the residual component.

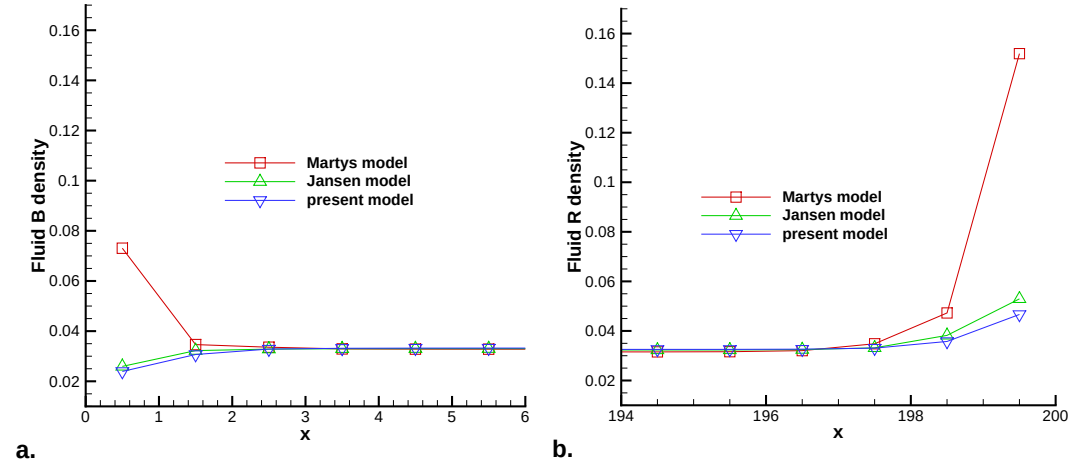


Figure 6: (Color online) The density profile of the residual fluid component near the wall along $y=50$. (a) The density profile of fluid B near the left wall. In this region, the wetting fluid R is the dominant component while the non-wetting fluid B is the residual component. (b) The density profile of fluid R near the right wall. In this region, the non-wetting fluid B is the dominant component while the wetting fluid R is the residual component.

fluid interactive forces acting on the fluid boundary nodes from surrounding fluid nodes. The Jansen model only adds the extra virtual fluid of the wetting component to the solid boundary nodes and keep the non-wetting component unchanged, while in the present model the extra virtual fluid is added to or subtracted from the wetting component or the non-wetting component on the solid boundary nodes at the same time, respectively, as shown in Eq. (2.12) and Eq. (2.13). As a result, the density variation in the Jansen model

https://doi.org/10.4208/cicp.101114.150415a Published online by Cambridge University Press

mainly appears on the non-wetting fluid (fluid B) region, while in the present model, the density variations evenly appears on the wetting fluid region and the non-wetting fluid region, as shown in Fig. 5 and Fig. 6. Although the density variations of the Jansen model in the wetting fluid region are smaller than the present model, the density variations of the Jansen model in the non-wetting fluid region are much larger than the present model. Therefore, the maximum non-physical effect caused by the density variations in the Jansen model should be larger than in the present model. Further comparisons will be presented in Section 3.4.

3.3 Problem with the particle suspension model with interior fluid

In this subsection, we will demonstrate numerically that the particle suspension model with interior fluid is not able to maintain mass conservation when the particle is penetrating the fluid interface, as we point out in Section 2.2.1.

The simulation domain is a 301×101 closed channel, with non-slip bounce-back boundary condition applied to the domain boundaries. The parameters of the fluid components are identical to the ones used in Section 3.1, except that the contact angle is set to be 90°. Thus, the effect of wetting models is minimized in this case, and we focus on the interior fluid of the particle model. As shown in Fig. 7, fluid B occupies the top half of the channel and fluid R occupies the bottom half of the channel. A round particle ($r=15$), is initially placed at $(50,50)$ inside the fluid B region, and the interior of the particle is filled with fluid B. The interior fluid will enter the LBM streaming-collision cycle, and the same bounce-back boundary condition applied to the interior fluid [26]. We move the particle with constant vertical velocity, $v=0.005$, towards the bottom of the channel, and monitor the total mass change of each fluid components outside the solid particle.

Fig. 7 shows significant shift of the fluid component composition inside the particle, despite that the particle is initially filled with pure fluid B. Although the total mass of each component in the whole domain, including the solid region, is strictly conserved for particle model with interior fluid, the fluid outside the solid region is not conserved and changes rapidly when the particle penetrates the fluid-fluid interface and enter fluid R region, as shown in Fig. 8. Meanwhile, when using particle model without interior fluid and using the virtual fluid method introduced in Section 2.1.2 to balance the interactive force on the fluid boundary nodes, the mass of each fluid component outside the particle is approximately conserved with some slight fluctuations when the particle is penetrating the fluid-fluid interface. Therefore, interior fluid is excluded in the rest of simulations in this paper.

3.4 Sedimentation of an elliptical particle

The impact of non-strictly immiscible nature of the Shan-Chen model and the non-physical effects caused by the wetting models on the particle motion should be investigated. However, once the fluid interface is involved, it is difficult to compare the multicomponent

https://doi.org/10.4208/cicp.101114.150415a Published online by Cambridge University Press

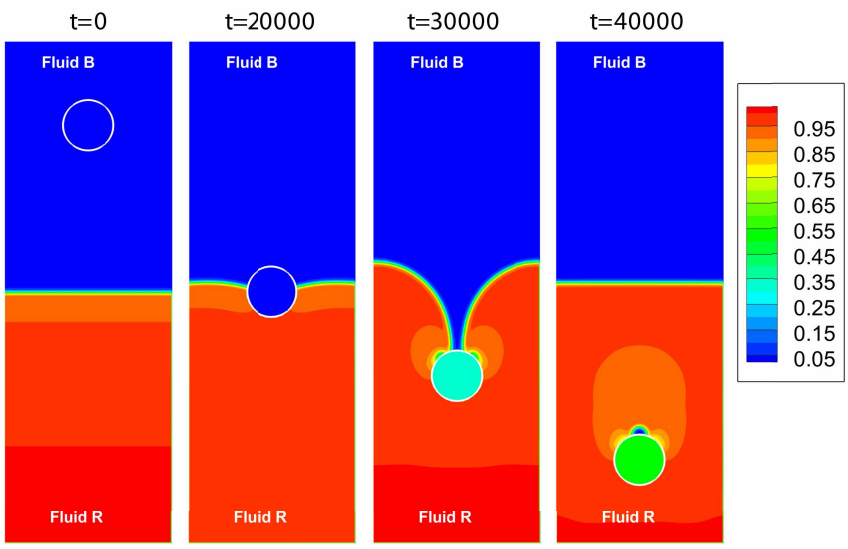


Figure 7: Contours of fluid R at different time (in lattice unit). After the particle penetrates the interface, some amount of fluid R enters the solid particle while some amount of fluid B leaks out of the particle and forms a small drop on the back of the particle.

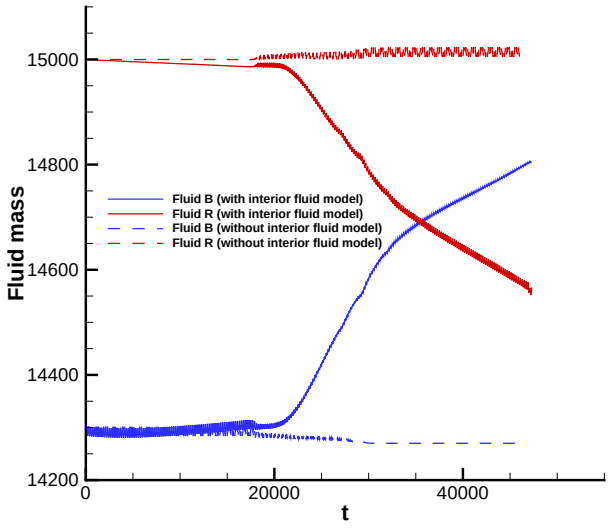


Figure 8: Total mass change of each fluid component outside the particle with time. The particle model with interior fluid cannot maintain mass conservation for fluid outside the particle, while the particle model excluding interior fluid can greatly reduce the mass nonconservation.

flow result with the well studied single phase flow result. When a particle is completely submerged in one fluid component, the particle motion should behave the same way as it is in the single phase fluid, as long as the particle is far away from the fluid interface. Therefore, we propose the following numerical simulations.

https://doi.org/10.4208/cicp.101114.150415a Published online by Cambridge University Press

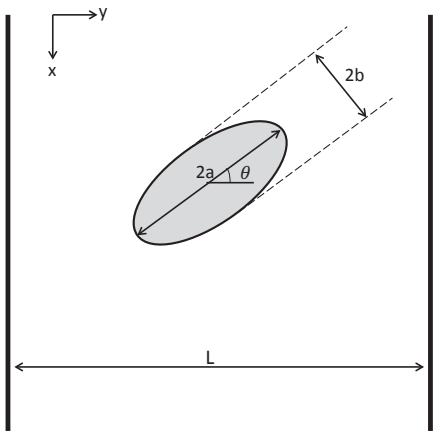


Figure 9: The geometry of the particle sedimentation benchmark case. a and b is the length of semi-major axis and semi-minor axis, respectively. L is the width of the channel. Gravity is along the x axis in the positive direction. θ represents the orientation of the particle.

The simulation domain is a 601×81 cavity, with non-slip bounce-back boundary condition applied on the domain boundaries. An elliptical particle is initially placed at $(60,40)$, as shown in Fig. 9. a and b is the length of semi-major axis and semi-minor axis, respectively. L is the width of the channel. Gravity is along the x axis in the positive direction. θ represents the orientation of the particle, and the initial value of θ is 135°. In lattice unit, $a=16$, $b=10$, and gravity is set to be 0.0001. Once released, the particle will sink under gravity. Except for some special cases (e.g., $\theta=0^\circ$ or $\theta=90^\circ$, and particle is initially located at the center of the channel), the particle will turn while sinking, leading to horizontal movement. The fluid parameters are the same with the ones used in Section 3.1. The density of the solid particle is 2.3, and the maximum Reynolds number is about 1.5.

3.4.1 Sedimentation in single phase fluid

First, we simulate the particle sedimentation in pure single phase fluid using our single phase code without introducing the Shan-Chen model. Fig. 10 shows the trajectory of the particle. There is negligible difference between the zeroth-order refill method and the first-order refill method in the single phase case, therefore only the single phase result with the first-order refill method will be used for comparison in the rest of the paper. In Ref. [11], we have validated our single phase code by comparing with the finite element method. Thus, result in Fig. 10 is reliable.

3.4.2 Sedimentation in multicomponent fluid

Second, we simulate the same sedimentation case above while this time we introduce the Shan-Chen model and the wetting models. In order to perform valid comparison with

https://doi.org/10.4208/cicp.101114.150415a Published online by Cambridge University Press

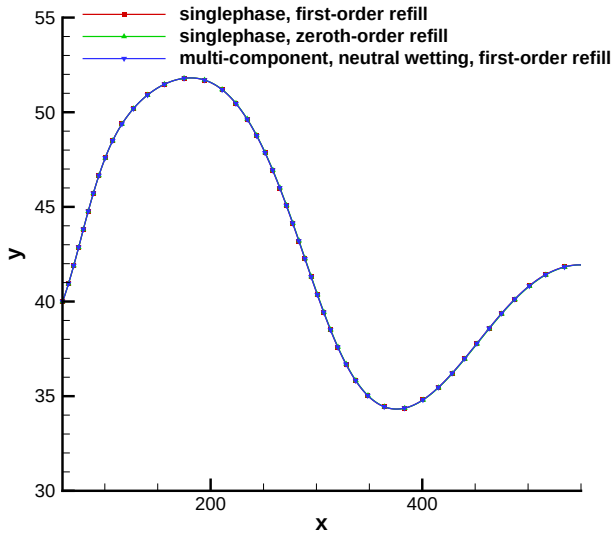


Figure 10: Trajectories of the particle, obtained by single phase code with first-order refill method, single phase code with first-order refill method and multicomponent code with neutral wetting and first-order refill method, respectively. The trajectories are almost identical for all three cases.

the result in Fig. 10, there should be no fluid-fluid interface or the interface should be far away from the particle. In this case, we remove the interface by fill the whole closed channel with one fluid component as the dominant component and a small amount of the other fluid component as the residual component, thus the slightly mixing feature of the Shan-Chen model is accounted for.

When the fluid-fluid interface exists, using the fluid parameters in Section 3.1, we find that the density of the average dominant fluid component is about 0.97, while the density of the residual fluid component is about 0.03. Thus, we use these two values as the initial density of the dominant component and the residual component, respectively.

We first focus on the slight mixing problem in the Shan-Chen model and let the two fluid components to be neutral wetting, resulting in 90° contact angle. Virtual fluid is used to balance the interactive forces on the fluid boundary nodes, so that the density variations near the fluid-solid boundaries are minimized. The multicomponent fluids result is almost identical to the single phase result, as shown in Fig. 10, despite that there is a small amount of residual component.

Now we further consider the effect of the wetting models. The contact angle is no longer 90°, and the parameters of the wetting models are listed in Table 1. We first set fluid R as the dominant fluid to simulate the situation when the particle is submerged in the wetting component. Then we set fluid B as the dominant fluid to simulate the situation when the particle is submerged in the non-wetting component. As already shown in Fig. 5 and Fig. 6, when the contact angle is not equal to 90°, density variations near the fluid-solid boundaries still exist even when the virtual fluid is used. Therefore, the effect

https://doi.org/10.4208/cicp.101114.150415a Published online by Cambridge University Press

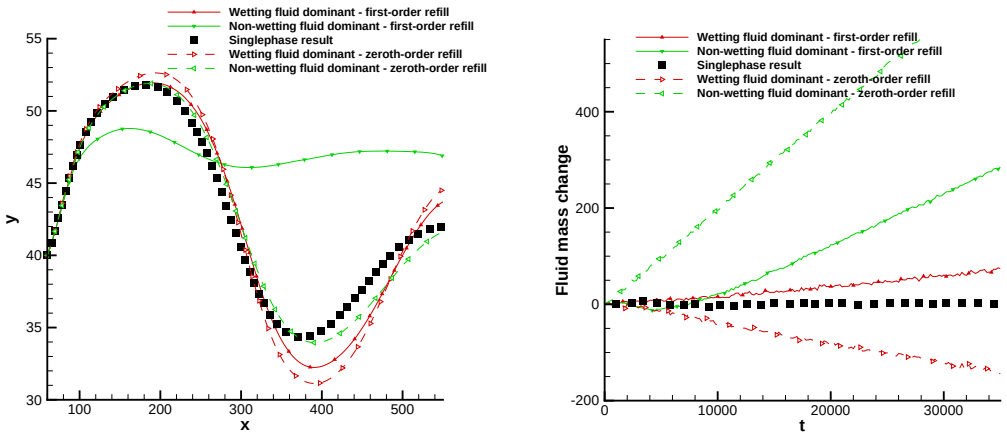


Figure 11: (Color online) Simulation results of an elliptical particle settling in a closed channel filled with wetting dominant component R with residual component B and non-wetting dominant component B with residual component R, respectively, using the Martys model. (a) Trajectories of the falling particle. (b) The fluid mass change of the dominant component outside the particle. The 'single phase' result is obtained by pure single phase LBM particle suspension code, excluding the Shan-Chen model and wetting models.

of the density variations as well as the fluid-solid interactive forces can be investigated here.

Fig. 11a shows the trajectories of the particle when the Martys model is adopted as the wetting model. We can see that the trajectories deviate significantly away from the single phase result, especially for the one using the first-order refill method in the non-wetting fluid region. Also, the fluid mass outside the particle is not conserved as shown in Fig. 11b. In the Martys model, no virtual fluid is used to balance the fluid-fluid interactive forces from neighboring fluid nodes on the boundary nodes, therefore the total net interactive force on the boundary nodes is the sum of the fluid-solid interactive forces and fluid-fluid interactive forces, which results in large density variations, as shown in Section 3.2. When the particle is submerged in the non-wetting fluid B, the residual wetting fluid R on the boundary nodes experiences especially high interactive forces from nearby nodes, because the fluid-fluid interactive forces and the fluid-solid interactive forces are both towards the solid surface, which results in very large density gradient near the solid surface, as shown in Fig. 6b. Thus, the density of the residual fluid R on the fluid node which is newly created by the first-order refill method is so much higher than the average density of the residual fluid R that at one point fluid components separation occurs and forms a small fluid R drop on the back of the particle, as shown in Fig. 12, which violates the assumption of no fluid-fluid interface.

Due to the large density variations caused by the Martys model, the present model and the Jansen model both utilize the virtual fluid to balance the fluid-fluid interactive forces on the boundary nodes, and on top of which the fluid-fluid interactive forces from the additional virtual fluid control the contact angle. As pointed out in Section 2.1.2, in

https://doi.org/10.4208/cicp.101114.150415a Published online by Cambridge University Press

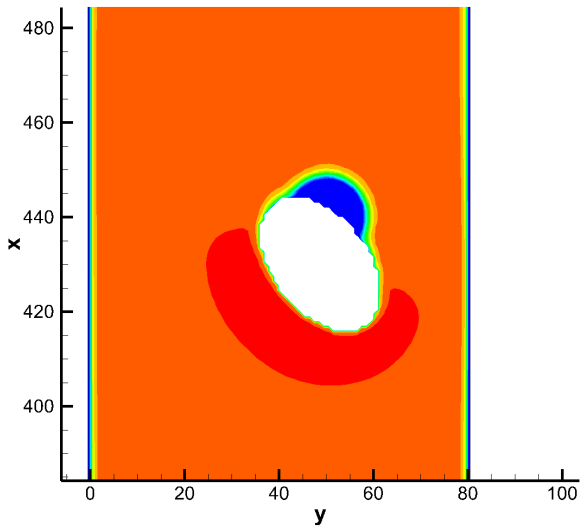


Figure 12: Contours of the density of fluid B (the non-wetting component). The particle is settling in fluid B dominant region using Martys model and first-order refill method. A small drop of fluid R is formed on the back of particle.

the Jansen model, only the virtual fluid density of the wetting component is modified which affects the interactive forces on the non-wetting component on the fluid boundary nodes, and therefore all the non-physical effects are concentrated on the non-wetting component region. As shown in Fig. 13a, the trajectories of particle in the wetting fluid component are almost identical to the single phase result, while in the non-wetting fluid component case the trajectories deviate away from the single phase result significantly. Fig. 13b shows the mass change of the dominant component with time. We can see that the fluid mass change is significant when using the zeroth-order refill method, while the fluid mass change is much smaller when using the first-order refill method. However, in the non-wetting component case, the fluid mass change is still significant for the Jansen model.

In the present model, the control of the virtual fluid density is more flexible, and the non-physical effects can be evenly distributed between the wetting component and the non-wetting component. As shown in Fig. 14a, the deviations of the trajectories in the multicomponent fluids from the single phase result are small for either the wetting component or the non-wetting component, and also the first-order refill method works a little better than the zeroth-order refill method. More dramatic improvement is found in mass conservation. In Fig. 14b, we can see that when the first-order refill method is used along with the present wetting model, the fluid mass of the dominant component is approximately conserved, meanwhile the fluid mass changes significantly when using the zeroth-order refill method. In Fig. 15a, the trajectories of the present model are directly compared with the trajectories of the Jansen model, and only the results obtained

https://doi.org/10.4208/cicp.101114.150415a Published online by Cambridge University Press

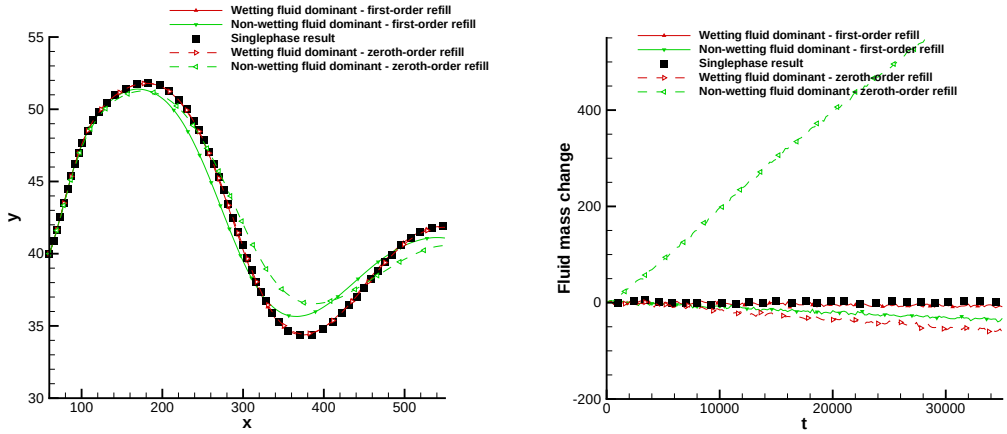


Figure 13: (Color online) Simulation results of an elliptical particle settling in a closed channel filled with wetting dominant component R with residual component B and non-wetting dominant component B with residual component R, respectively, using the Jansen model. (a) Trajectories of the falling particle. (b) The fluid mass change of the dominant component outside the particle. The 'single phase' result is obtained by pure single phase LBM particle suspension code, excluding the Shan-Chen model and wetting models.

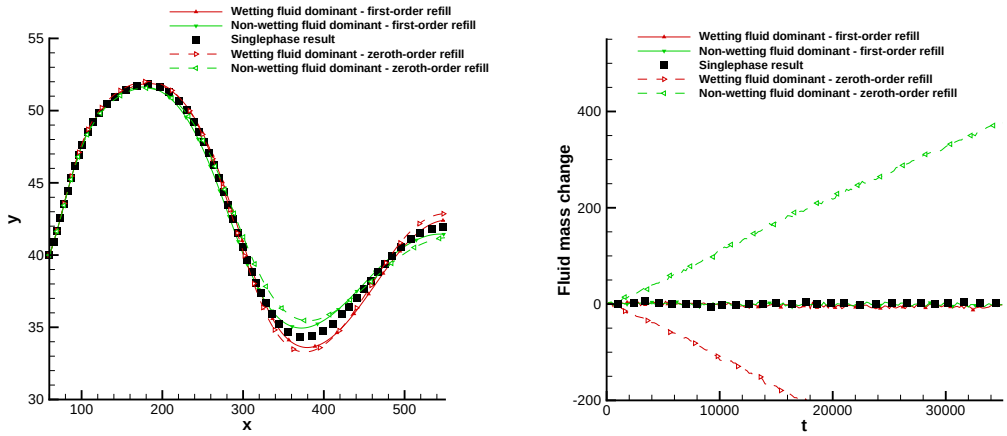


Figure 14: (Color online) Simulation results of an elliptical particle settling in a closed channel filled with wetting dominant component R with residual component B and non-wetting dominant component B with residual component R, respectively, using the present model. (a) Trajectories of the falling particle. (b) The fluid mass change of the dominant component outside the particle. The 'single phase' result is obtained by pure single phase LBM particle suspension code, excluding the Shan-Chen model and wetting models.

using the first-order refill method are shown. The maximum deviation from the single phase result occurs in the non-wetting component case using the Jansen model, thus, the overall accuracy of the present model is higher than the overall accuracy of the Jansen model. Also, the total mass of the dominant component is approximately conserved in

https://doi.org/10.4208/cicp.101114.150415a Published online by Cambridge University Press

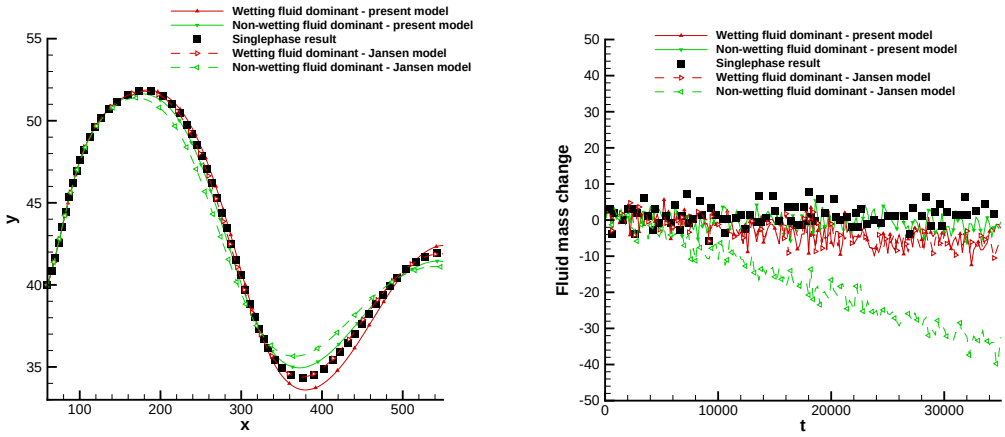


Figure 15: (Color online) Comparison of simulation results obtained by the present model and the Jansen model, using the first-order refill method. (a) Trajectories of the falling particle. (b) The fluid mass change of the dominant component outside the particle. The maximum deviation of the trajectory from the single phase result occurs when the particle is settling in non-wetting fluid using the Jansen model. The mass is approximately conserved for the present model, while the mass is not conserved for the Jansen model when the particle is in non-wetting component.

the present model while the total mass of non-wetting component decreases in the Jansen model, as shown in Fig. 15b.

Fig. 16 shows the vectors of the fluid-fluid interactive force acting on the dominant fluid component on the fluid nodes near the particle. Consistent with our analysis, the fluid-solid interactive force which is used to control the contact angle is mainly concentrated in the non-wetting component in the Jansen model, while in the present model, the fluid-solid interactive force is evenly distributed in each component. As a result, the overall influence of the discretized fluid-solid interactive forces to the suspended particle is smaller in the present model than in the Jansen model.

3.5 Particle penetrating the fluid interface

In Section 3.4 we considered the multicomponent effects to the particle with the absence of the fluid interface and monitored the fluid mass drift for each component. In this subsection, we will focus on the process of the particle penetrating the fluid interface and monitor the fluid mass drift.

The simulation configuration is identical to the one in Section 3.3, except that the fluid R is the wetting phase and fluid B is the non-wetting phase and the interior fluid is excluded, as shown in Fig. 17. The wetting parameters of the fluids are chosen from Table 1. Since the zero-order refill method results in significant fluid mass drift for all three wetting models, as shown in Fig. 11, Fig. 13 and Fig. 14, here we only perform the simulations with the first-order refill method.

We monitor the fluid mass drift for each component, and the results are shown in

https://doi.org/10.4208/cicp.101114.150415a Published online by Cambridge University Press

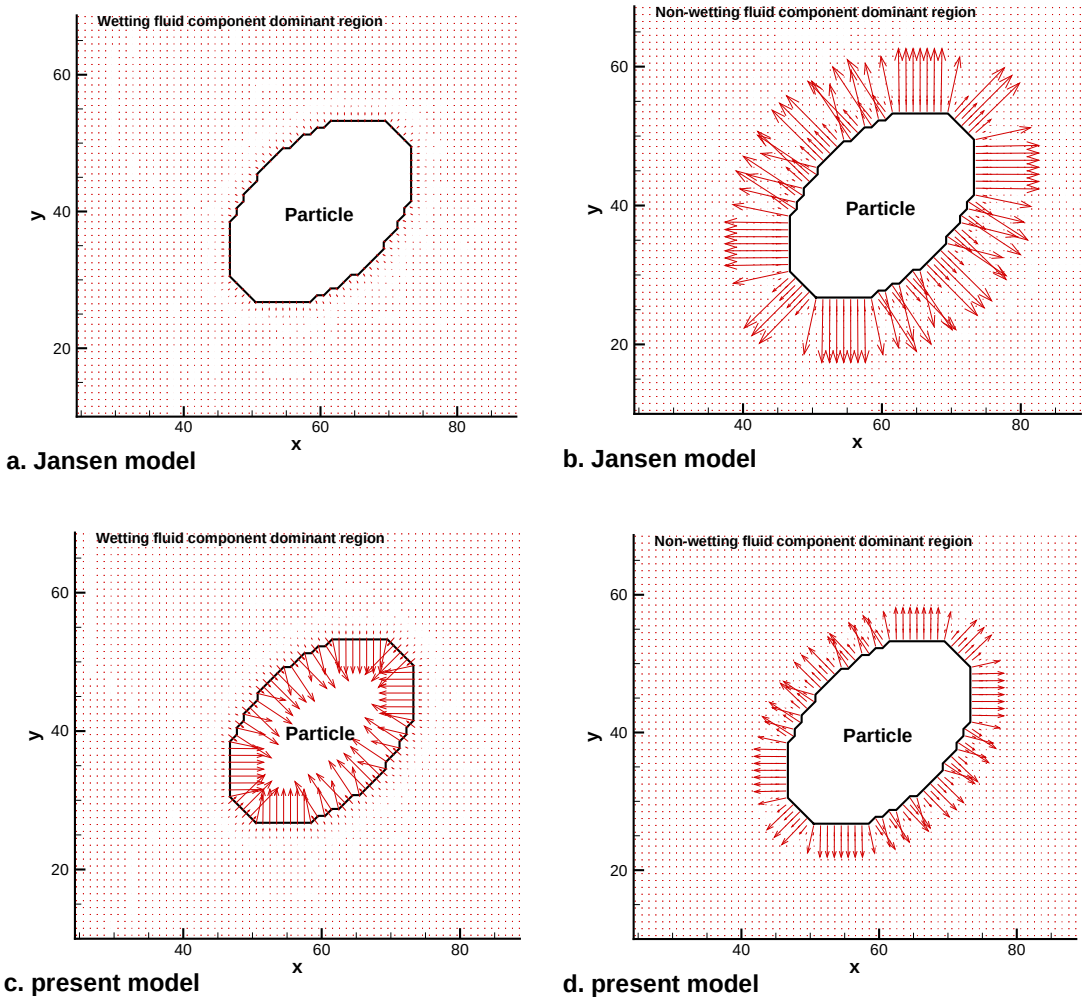


Figure 16: Vectors of the fluid-fluid interactive force acting on the dominant fluid component on the fluid nodes near the particle.

Fig. 18. The Martys model performs the worst among the three models. The present model works equally well before and after the interface penetration. The nonwetting phase mass drift before penetration is very close to the wetting phase mass drift after penetration. For the Jansen model, because most of the nonphysical effects are concentrated in the nonwetting phase, the nonwetting phase mass drift before penetration is very large, resulting in a high peak before penetration as shown in Fig. 18, although the wetting phase mass drift is slightly smaller than the present model after penetration.

In summary, the present approach has the overall lowest level of maximum mass drift during the whole process of the penetration. The remaining small mass drift can be corrected by evenly redistributing the extra mass to the solid surface [31].

https://doi.org/10.4208/cicp.101114.150415a Published online by Cambridge University Press

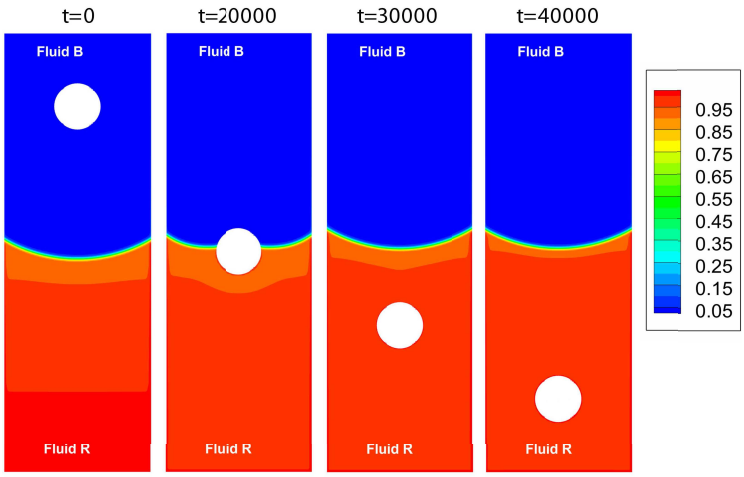


Figure 17: Contours of fluid R at different time (in lattice unit). Fluid R is the wetting phase, while fluid B is the nonwetting phase.

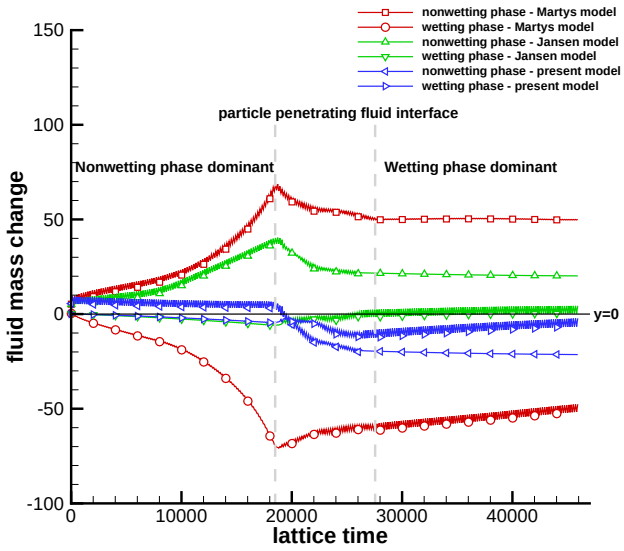


Figure 18: Fluid mass variation of each fluid component outside the particle with time. The first-order refill method is used here. The present model has the lowest level of the maximum mass drift in the overall particle settling process.

3.6 Particle suspended on the fluid interface

In this subsection, we perform three dimensional simulations of particle suspended on fluid interface. For the problem shown in Fig. 3, the fluid-solid interactive forces induced by the wetting model determine the final shape of the fluid drop, and the contact an-

https://doi.org/10.4208/cicp.101114.150415a Published online by Cambridge University Press

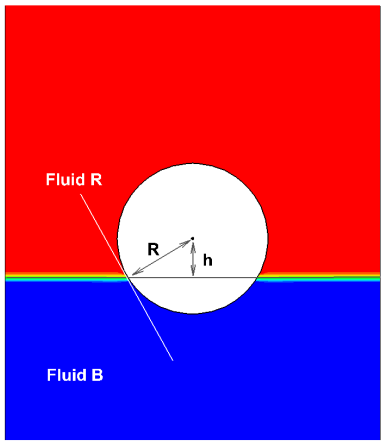


Figure 19: A schematic illustration of calculating contact angle based on the equilibrium position of a spherical particle suspended on the fluid interface.

gles are formed by a flat solid surface in contact with these two fluid components. For the problem of a particle suspending on the interface of two fluid components shown in Fig. 19, if gravity is neglected, the fluid-solid interactive forces determine the stable position of the particle, and hence the final static contact angles. If the wetting model is correct and all the corresponding LBM parameters used in both simulations are the same, then the static contact angles predicted from both cases should be consistent with each other.

As shown in Fig. 19. The contact angle can be obtained by measuring the distance h between the particle center and the interface surface. Then the contact angle of fluid R is,

$$\theta_R = \arccos\left(\frac{h}{R}\right). \tag{3.3}$$

The computation grid used here is $130\times128\times128$, with bounce-back boundary condition applied to $x=1$ and $x=130$, and periodic boundary condition applied to other boundary planes. Other parameters in LBM are identical to the ones used in Section 3.1. Initially, a spherical particle with a radius of 15 in lattice unit is placed in the center of the simulation domain. The density of the particle is 2 in lattice unit. For $x\leq65$, the domain is filled with fluid R, while for For $x\geq66$ the domain is filled with fluid B. If the contact angle for fluid R and B is 90°, then the initial particle position is the equilibrium position.

As we adjust the wetting parameters of our wetting model, the particle will not be balanced by the wetting force in its initial position. After the particle reached to its equilibrium position, we then measured the position of the particle center and the position of fluid interface, and calculated the contact angle according to Fig. 19 and Eq. (3.3). Meanwhile, we also obtain the value of contact angle according to Fig. 3 and Eq. (3.2). We then compared the contact angle obtained by the above two methods. As shown in Fig. 20,

https://doi.org/10.4208/cicp.101114.150415a Published online by Cambridge University Press

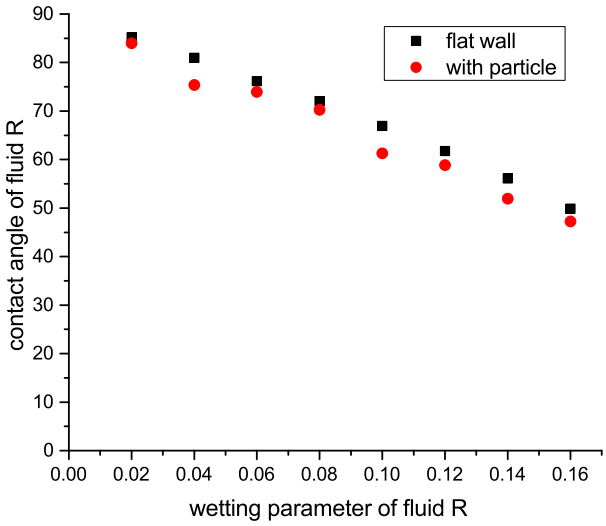


Figure 20: Comparisons of contact angles obtained by 3D simulations of a drop attached to a flat wall and 3D simulations of a particle suspended on the fluid interface.

we can see that the contact angles obtained by these two methods are very close to each other, which indicates that our proposed wetting model is correct. The value of the wetting parameter of fluid B is the opposite number of fluid R in Fig. 20, as suggested in Section 2.1.2.

The contact angles obtained by particle suspended on the interface experience some fluctuations, and also, the obtained contact angles with particle are slightly smaller than the ones with flat wall. The zigzag representation of the curved surface of the particle, as well as the compressible effect of LBM, may be responsible for the small deviations. By increasing the grid resolution, we are able to obtain better consistency between these two contact angle measurement methods.

4 Conclusions

In this work, the impact of non-physical density variations near the solid surface, caused by introduction of the wetting models in the Shan-Chen lattice Boltzmann multicomponent model, on the particle motion in binary immiscible fluids is studied. A modified wetting model combined with the first-order refill method is then proposed to reduce the non-physical effects, and the performance of the new approach is evaluated by comparison with existing wetting models.

Our numerical results show that the density variations caused by the combined effect of the weak compressibility and wetting models can affect the motion of the suspended particle significantly. Although the Jansen model can eliminate such variations for fluids of neutral wetting, it still leads to relatively large density variations near the surface of the

https://doi.org/10.4208/cicp.101114.150415a Published online by Cambridge University Press

solid phase in the non-wetting fluid phase while there are negligible density variations in the wetting phase. The wetting model proposed in this study can keep the magnitude of the density variations in the same relatively low level for both the wetting phase and the non-wetting phase. As a result, the overall accuracy can be improved.

The refill method used to reconstruct fluid information in the newly created lattice nodes when the particle moves away plays a much more important role in ensuring fluid mass conservation here than in the single phase case, due to the fluid density variations mentioned above near the solid surface, as shown in our simulations. The first-order refill method which considers the gradient of the density variations can significantly improve the fluid mass conservation during the settling process of the particle, especially when combined with the present wetting model. The extra computation cost for the first-order refill method is negligible compared with the overall computation cost, as the refill procedure only occurs when the particle moves to uncover fluid nodes. Also, the refill procedure mostly occurs near the rear edge of the particle where there are usually enough fluid nodes for extrapolations used in the first-order refill method.

In summary, our modified wetting model, combined with the first-order refill method, significantly improves mass conservation and simulation accuracy, no matter whether the particle is submerged in one component (Fig. 15) or penetrating fluid interface (Fig. 18). In addition, the present approach has the overall lowest level of fluid mass drift during the whole process of the particle penetrating the fluid interface.

We do notice that when the contact angle is very large or small, or the surface tension is very large, the interactive forces between solid and fluid can be relatively large and result in large density variations near the solid surface. In such case, a small amount of fluid mass change still exists even using our approach. The process of the particle penetrating the fluid-fluid interface will also cause a small amount of fluid mass change. However, compared with previous approaches, the fluid mass drift is significantly reduced in the present approach. In these cases, one can just monitor the fluid mass drift, and redistribute the extra mass on the particle surface. We suggest that the evaluation of the extra mass should be averaged over time but not every step, since some mass fluctuations are caused by the change of lattice nodes occupied by the particle, and once the averaged extra mass reaches a threshold the redistribution procedure is then carried out.

Acknowledgments

This work is financially supported by the NSFC grants (No. 51176089 and No. 11221061), the Key Basic Scientific Research Program (2013CB228301), and Specialized Research Fund for the Doctoral Program of Higher Education of China (No. 20130002110077). M. Wang acknowledges the support from Tsinghua University Initiative Scientific Research Program (No. 2014z22074). Y. Chen acknowledges the support of National Science Foundation for Postdoctoral Scientists of China (Grant No. 2014M550716). Q. Kang acknowledges the support of LANLs LDRD Program.

https://doi.org/10.4208/cicp.101114.150415a Published online by Cambridge University Press

References

[1] C. K. Aidun and J. R. Clausen. Lattice-Boltzmann method for complex flows. *Annual Review of Fluid Mechanics*, 42:439–472, 2010.

[2] C. K. Aidun, Y. N. Lu, and E. J. Ding. Direct analysis of particulate suspensions with inertia using the discrete Boltzmann equation. *Journal of Fluid Mechanics*, 373:287–311, 1998.

[3] S. Arditty, C. P. Whitby, B. P. Binks, V. Schmitt, and F. Leal-Calderon. Some general features of limited coalescence in solid-stabilized emulsions. *The European Physical Journal E*, 11(3):273–281, 2003.

[4] B. P. Binks. Particles as surfactants – similarities and differences. *Current Opinion in Colloid & Interface Science*, 7(1C2):21–41, 2002.

[5] M. Bouzidi, M. Firdaouss, and P. Lallemand. Momentum transfer of a Boltzmann-lattice fluid with boundaries. *Physics of Fluids*, 13(11):3452–3459, 2001.

[6] A. Caiazzo and M. Junk. Boundary forces in lattice Boltzmann: Analysis of momentum exchange algorithm. *Computers & Mathematics with Applications*, 55(7):1415–1423, 2008.

[7] H. D. Chen, S. Y. Chen, and W. H. Matthaeus. Recovery of the navier-stokes equations using a lattice-gas Boltzmann method. *Physical Review A*, 45(8):R5339–R5342, 1992.

[8] L. Chen, Q. Kang, Y. Mu, Y.-L. He, and W.-Q. Tao. A critical review of the pseudopotential multiphase lattice Boltzmann model: Methods and applications. *International Journal of Heat and Mass Transfer*, 76(0):210–236, 2014.

[9] S. Chen and G. D. Doolen. Lattice Boltzmann method for fluid flows. *Annual Review of Fluid Mechanics*, 30:329–364, 1998.

[10] S. Y. Chen, D. Martinez, and R. W. Mei. On boundary conditions in lattice Boltzmann methods. *Physics of Fluids*, 8(9):2527–2536, 1996.

[11] Y. Chen, Q. Cai, Z. Xia, M. Wang, and S. Chen. Momentum-exchange method in lattice Boltzmann simulations of particle-fluid interactions. *Physical Review E*, 88(1):013303, 2013.

[12] B. Chun and A. J. C. Ladd. Interpolated boundary condition for lattice Boltzmann simulations of flows in narrow gaps. *Physical review E*, 75(6):066705, 2007.

[13] J. R. Clausen and C. K. Aidun. Galilean invariance in the lattice-Boltzmann method and its effect on the calculation of rheological properties in suspensions. *International Journal of Multiphase Flow*, 35(4):307–311, 2009.

[14] B. K. Cook, D. R. Noble, and J. R. Williams. A direct simulation method for particle-fluid systems. *Engineering Computations*, 21(2-4):151–168, 2004.

[15] I. Ginzburg and D. d'Humières. Multireflection boundary conditions for lattice Boltzmann models. *Physical Review E*, 68(6):066614, 2003.

[16] F. Günther, F. Janoschek, S. Frijters, and J. Harting. Lattice Boltzmann simulations of anisotropic particles at liquid interfaces. *Computers & Fluids*, 80:184–189, 2013.

[17] Z. Guo, B. Shi, and N. Wang. Lattice BGK model for incompressible Navier-Stokes equation. *Journal of Computational Physics*, 165(1):288–306, 2000.

[18] Z. Guo, C. Zheng, and B. Shi. Discrete lattice effects on the forcing term in the lattice Boltzmann method. *Physical Review E*, 65(4):046308, 2002.

[19] X. Y. He and L. S. Luo. Lattice Boltzmann model for the incompressible Navier-Stokes equation. *Journal of Statistical Physics*, 88(3-4):927–944, 1997.

[20] E. M. Herzig, A. Robert, D. D. van't Zand, L. Cipelletti, P. N. Pusey, and P. S. Clegg. Dynamics of a colloid-stabilized cream. *Physical Review E*, 79(1):011405, 2009.

[21] R. Holtzman, M. L. Szulczewski, and R. Juanes. Capillary fracturing in granular media. *Physical Review Letters*, 108(26):264504, 2012.

https://doi.org/10.4208/cicp.101114.150415a Published online by Cambridge University Press

[22] S. L. Hou, X. W. Shan, Q. S. Zou, G. D. Doolen, and W. E. Soll. Evaluation of two lattice Boltzmann models for multiphase flows. *Journal of Computational Physics*, 138(2):695–713, 1997.
[23] F. Jansen and J. Harting. From bijels to Pickering emulsions: A lattice Boltzmann study. *Physical Review E*, 83(4):046707, 2011.
[24] A. S. Joshi and Y. Sun. Multiphase lattice Boltzmann method for particle suspensions. *Phys Rev E Stat Nonlin Soft Matter Phys*, 79(6 Pt 2):066703, 2009.
[25] Q. J. Kang, D. X. Zhang, and S. Y. Chen. Displacement of a two-dimensional immiscible droplet in a channel. *Physics of Fluids*, 14(9):3203–3214, 2002.
[26] A. J. C. Ladd. Numerical simulations of particulate suspensions via a discretized Boltzmann-equation. 1. Theoretical foundation. *Journal of Fluid Mechanics*, 271:285–309, 1994.
[27] P. Lallemand and L. S. Luo. Lattice Boltzmann method for moving boundaries. *Journal of Computational Physics*, 184(2):406–421, 2003.
[28] G. Liang, Z. Zeng, Y. Chen, J. Onishi, H. Ohashi, and S. Chen. Simulation of self-assemblies of colloidal particles on the substrate using a lattice Boltzmann pseudo-solid model. *Journal of Computational Physics*, 248(0):323–338, 2013.
[29] N. S. Martys and H. Chen. Simulation of multicomponent fluids in complex three-dimensional geometries by the lattice Boltzmann method. *Physical Review E*, 53(1):743, 1996.
[30] R. W. Mei, L. S. Luo, and W. Shyy. An accurate curved boundary treatment in the lattice Boltzmann method. *Journal of Computational Physics*, 155(2):307–330, 1999.
[31] N. Q. Nguyen and A. J. C. Ladd. Lubrication corrections for lattice-Boltzmann simulations of particle suspensions. *Physical Review E*, 66(4):046708, 2002.
[32] J. Onishi, A. Kawasaki, Y. Chen, and H. Ohashi. Lattice Boltzmann simulation of capillary interactions among colloidal particles. *Computers & Mathematics with Applications*, 55(7):1541–1553, 2008.
[33] M. L. Porter, E. T. Coon, Q. Kang, J. D. Moulton, and J. W. Carey. Multicomponent interparticle-potential lattice Boltzmann model for fluids with large viscosity ratios. *Physical Review E*, 86(3):036701, 2012.
[34] D. W. Qi. Lattice-Boltzmann simulations of particles in non-zero-reynolds-number flows. *Journal of Fluid Mechanics*, 385:41–62, 1999.
[35] Y. H. Qian, D. d'Humières, and P. Lallemand. Lattice BGK models for Navier-Stokes equation. *Europhysics Letters*, 17(6bis):479–484, 1992.
[36] A. R. Rickards, H. D. Brannon, W. D. Wood, et al. High strength ultralightweight proppant lends new dimensions to hydraulic fracturing applications. *SPE Production & Operations*, 21(02):212–221, 2006.
[37] M. Sbragaglia, R. Benzi, L. Biferale, S. Succi, K. Sugiyama, and F. Toschi. Generalized lattice Boltzmann method with multirange pseudopotential. *Physical Review E*, 75(2):026702, 2007.
[38] X. W. Shan and H. D. Chen. Lattice Boltzmann model for simulating flows with multiple phases and components. *Physical Review E*, 47(3):1815–1819, 1993.
[39] X. W. Shan and H. D. Chen. Simulation of nonideal gases and liquid-gas phase-transitions by the lattice Boltzmann-equation. *Physical Review E*, 49(4):2941–2948, 1994.
[40] X. W. Shan and G. Doolen. Multicomponent lattice-Boltzmann model with interparticle interaction. *Journal of Statistical Physics*, 81(1-2):379–393, 1995.
[41] K. Stratford, R. Adhikari, I. Pagonabarraga, and J. C. Desplat. Lattice Boltzmann for binary fluids with suspended colloids. *Journal of Statistical Physics*, 121(1-2):163–178, 2005.
[42] K. Stratford, R. Adhikari, I. Pagonabarraga, J. C. Desplat, and M. E. Cates. Colloidal jamming at interfaces: A route to fluid-bicontinuous gels. *Science*, 309(5744):2198–201, 2005.

https://doi.org/10.4208/cicp.101114.150415a Published online by Cambridge University Press

[43] M. Wang and Q. Kang. Modeling electrokinetic flows in microchannels using coupled multiple lattice Boltzmann methods. *J. Comput. Phys.*, 229(1):728–744, 2010.
[44] M. Wang, J. K. Wang, and S. Y. Chen. Roughness and cavitations effects on electro-osmotic flows in rough microchannels using the lattice poisson-Boltzmann methods. *J. Comput. Phys.*, 226(1):836–851, 2007.
[45] B. Wen, C. Zhang, Y. Tu, C. Wang, and H. Fang. Galilean invariant fluidcsolid interfacial dynamics in lattice Boltzmann simulations. *Journal of Computational Physics*, 266:161–170, 2014.
[46] Z. Xia, K. W. Connington, S. Rapaka, P. Yue, J. J. Feng, and S. Chen. Flow patterns in the sedimentation of an elliptical particle. *Journal of Fluid Mechanics*, 625:249, 2009.
[47] X. Yin and J. Zhang. An improved bounce-back scheme for complex boundary conditions in lattice Boltzmann method. *Journal of Computational Physics*, 231(11):4295–4303, 2012.
[48] D. Yu, R. Mei, and W. Shyy. A unified boundary treatment in lattice Boltzmann method. *New York: AIAA*, 953:2003, 2003.
[49] Q. S. Zou, S. L. Hou, S. Y. Chen, and G. D. Doolen. An improved incompressible lattice Boltzmann model for time-independent flows. *Journal of Statistical Physics*, 81(1-2):35–48, 1995.

https://doi.org/10.4208/cicp.101114.150415a Published online by Cambridge University Press